SUPPLEMENTARY FIGURES AND MOVIE LEGENDS

Supplementary Figure 1: GFAP positive nerves in patients with adenocarcinoma of the pancreas.

(A) Images of nerves stained for GFAP (green), S100 (red) and DAPI (blue), from patients with pancreatic adenocarcinomas, that score moderately (+) or highly (++) for GFAP. Scale bar: 50μm. (B) Table showing pathology reports of the 10 patients. (B) Images of an highly infiltrated nerve with GFAP (green) and S100 (red) staining, and corresponding H&E, showing almost complete disappearance of nerve tissue. Scale bar: 100μm.

Supplementary Figure 2:GFAP+ Schwann cells are associated with cancer cells in vivo (human and mice specimen)

(A) GFAP+ Schwann cells are associated with cancer cells in a fragment of the facial nerve of a patient with salivary duct carcinoma. Scale bar: 50 μm. (B) GFAP+ Schwann cells are associated with cancer cells in a fragment of the infraorbital nerve of a patient with skin squamous cell carcinoma. Scale bar: 50 μm. (C) GFAP+ Schwann cells wrap individual cancer cells in a fragment of the recurrent laryngeal nerve of a patient with thyroid cancer. Scale bar: 20 μm. (D) Myelin Protein Zero+ Schwann cells are not associated with cancer cells in the patient with thyroid cancer. Scale bar: 50 μm. (E) GFAP+ Schwann cells with long processes are associated with injected MiaPaCa-2 cancer cells in a murine sciatic nerve. Scale bars: 50 μm.

Supplementary Figure 3: Schwann cells are present along neurites in DRG and are not required for neurite growth. (A) Immunofluorescence staining for GFAP (green) and Tuj1 (red). The full arrow marks a neuron element and the arrowhead marks a Schwann cell. Scale bars are 200 μm (upper image) and 20 μm (lower image). (B) Time lapse observations of a radiated DRG showing neurite growth. Images were taken every 5 min for 24h by phase contrast. Time is hours: minutes. Scale bar is 30 μm.

Supplementary Figure 4: Expression of Schwann cell markers in HEI-286 cells. HEI-286 cells express both markers of Schwann cells involved in nerve repair (GFAP and p75) and markers of Schwann cells involved in myelination (MBP and MPZ). Immunofluorescence staining of GFAP, p75, MBP, and MPZ with nuclei staining (DAPI). Scale bars: 100 μm.

Supplementary Figure 5: Reorganization of cancer cell clusters

(A) Panc1 cancer cell clusters reorganize in presence of Schwann cells. Microscopic examination of organization of Panc1 cancer cells grown in Matrigel together with Schwann cells. Quantification of cancer cell reorganization using the shape factor index for Panc1 clusters growing with (HEI) or without (No HEI) HEI-286 Schwann cells. Data are means ± SEM. Significance was determined using t test (****$p<0.0001$, n (No HEI)=9, n (HEI)=7). (B) Microscopic examination of MiaPaCa-2 cell organization in Matrigel with NIH3T3. The cancer cell cluster shape is unaffected by contact with NIH3T3 (See quantification in Figure 6). Scale bars: 50 μm.

Supplementary Figure 6: Schwann cells form tunnels in Matrigel.

(A) Time lapse images showing the formation of tunnels in Matrigel by the HEI-286 Schwann cell line. Arrow indicates tunnel after retraction of Schwann cells. Times are hours:minutes. (B) Puromycin treatment (3μg/ml) does not impair cancer invasion of puromycin resistant MiaPaCa-2 cancer cells in presence of puromycin resistant HEI-286 Schwann cell (control n=4, puromycin n=7, ns, t test). (C) Removal of non-puromycin resistant Schwann cells by puromycin treatment generates intact, empty tunnels. Immunofluorescence staining for laminin (red) and HEI-286 (F-GFP) in Matrigel samples that were mock (upper panels) or puromycin treated (lower panels). Small white arrows show empty tunnels, long arrow shows a tunnel with Schwann cells. Brightfield images (right) indicate absence or remnants (black arrow) of Schwann cells at location of tunnels. Scale bars: 50 μm.

Supplementary Figure 7: Characterization of NCAM depleted HEI-286 Schwann cells.

(A) Immunofluorescence staining for NCAM in control (sh) and NCAM depleted (sh NCAM1) HEI-286 cells. Scale bar: 20 μm. (B). Cell proliferation of control (sh), and NCAM depleted (shNCAM1 and shNCAM2) HEI-286 cells. Data are mean ± SD, n=3 for each data point. (C) Quantification of velocity of control (sh cont) and NCAM depleted (shNCAM) HEI-286 cells. Cells were seeded in insert (Ibidi) for 24h and allowed to migrate after removal of the insert. Velocity was calculated after measuring distance covered over a 24h period. Data are means ± SEM, n=7 for each cell type. Difference was not found significant, as determined using t test.

Supplementary Figure 8: Overexpression of NCAM in NIH 3T3 fibroblasts grown in Matrigel does not affect MiaPaCa-2 cells invasion.

Quantification of MiaPaCa-2 invasion in Matrigel grown with NIH 3T3 overexpressing NCAM or not. Data are means ± SEM, n=16 for each condition (2 experiments). No significant difference was found, as determined using t test. Microscopic images show overexpression of NCAM in 3T3 cells. Scale bar = 100μm.

Supplementary Figure 9: NCAM depletion in Schwann cells reduced cancer cell recruitment to neurites of irradiated DRGs.

Irradiated DRGs were rescued with shNCAM HEI-286 (50,000cells) vs shcontrol HEI-286 6 days post radiation treatment, followed by the additional of MiaPaCa-2 cancer cells (50,000 cells) on day 7. Microscopic examination of the recruitment of cancer cells (red) to radiated DRGs and NCAM depleted Schwann cells (green). Images show MiaPaCa-2 (F-RFP) and HEI-286 (F-GFP) and were taken 10 days post irradiation. Quantification of the percentage of cancer cells that associated with the neurites in the presence of shC (n=13) and sh2 (n=16). Data are mean ± SEM. *P<0.05, **P<0.001, t test. Scale bars: 100μm.

MOVIES:

Movie S1. Time lapse of DRG and MiaPaCa-2 (expressing F-RFP) co-cultures. (A) MiaPaCa-2 cells move along neurites toward the center of the DRG. (B) Association of a

Schwann cell and cancer cell during cancer cell migration.(C) A cluster of cancer cells approaching a neurite projection via an association (bridge) with Schwann cells. (D) A cluster of cancer cells that are not directed to a neurite projection (control for cells from movie C). Images were taken every 5 min for 24h by phase contrast and fluorescence microscopy. Time is hours:minutes. Scale bars are 30 μm.

Movie S2. **Time lapse observations of MiaPaCa-2 (F-RFP) and Schwann cells (HEI-286 F-GFP) in 3D Matrigel**. (A) Formation of a chain of cancer cells (red) in contact with Schwann cells (green) (See figure 5B). (B) Isolation of a single cell from a cluster of cancer cells (red). Note that this cancer cell is constantly in contact with a Schwann cell (green) during the dissociation of the cancer cell from its cluster (See figure 5B). Images were taken every 5 min for 24h by fluorescence microscopy. Time is hours: minutes. Scale bars are 30 μm

Movie S3. **Time lapse observations of MiaPaCa-2 (F-RFP) and Schwann cells (HEI-286 F-GFP) grown on top of Matrigel.** (A) MiaPaCa-2 cells (red) grow as a cluster. Scale bar is 60μm. Compare with B. (See figure 6A). (B) In the presence of Schwann cells, MiaPaCa-2 cells dissociate from the cluster. The dissociated cancer cell is constantly in contact with Schwann cells. Scale bar is 60μm. Compare with movie A (See figure 6A). (C) Intercalation of Schwann cells between MiaPaCa-2 cells before the dissociation of a cancer cell from its cluster. Note the protrusion of the Schwann cells intercalating between cancer cells and the loss of strong contact between cancer cells. Scale bar is 60 μm (See figure 6B-D). (D) Formation of a cancer cell protrusion after

contact with a Schwann cell. Scale bar is 80μm. (See Figure 6D). (E) Sequential events: cancer cell protrusion, Schwann cell intercalation and cancer cell migration after hetero-cellular contact Schwann cell-cancer cell. Scale bar is 80μm (See Figure 6D). Images were taken every 5 min for 24h by phase contrast and fluorescence microscopy. Time is hours:minutes.

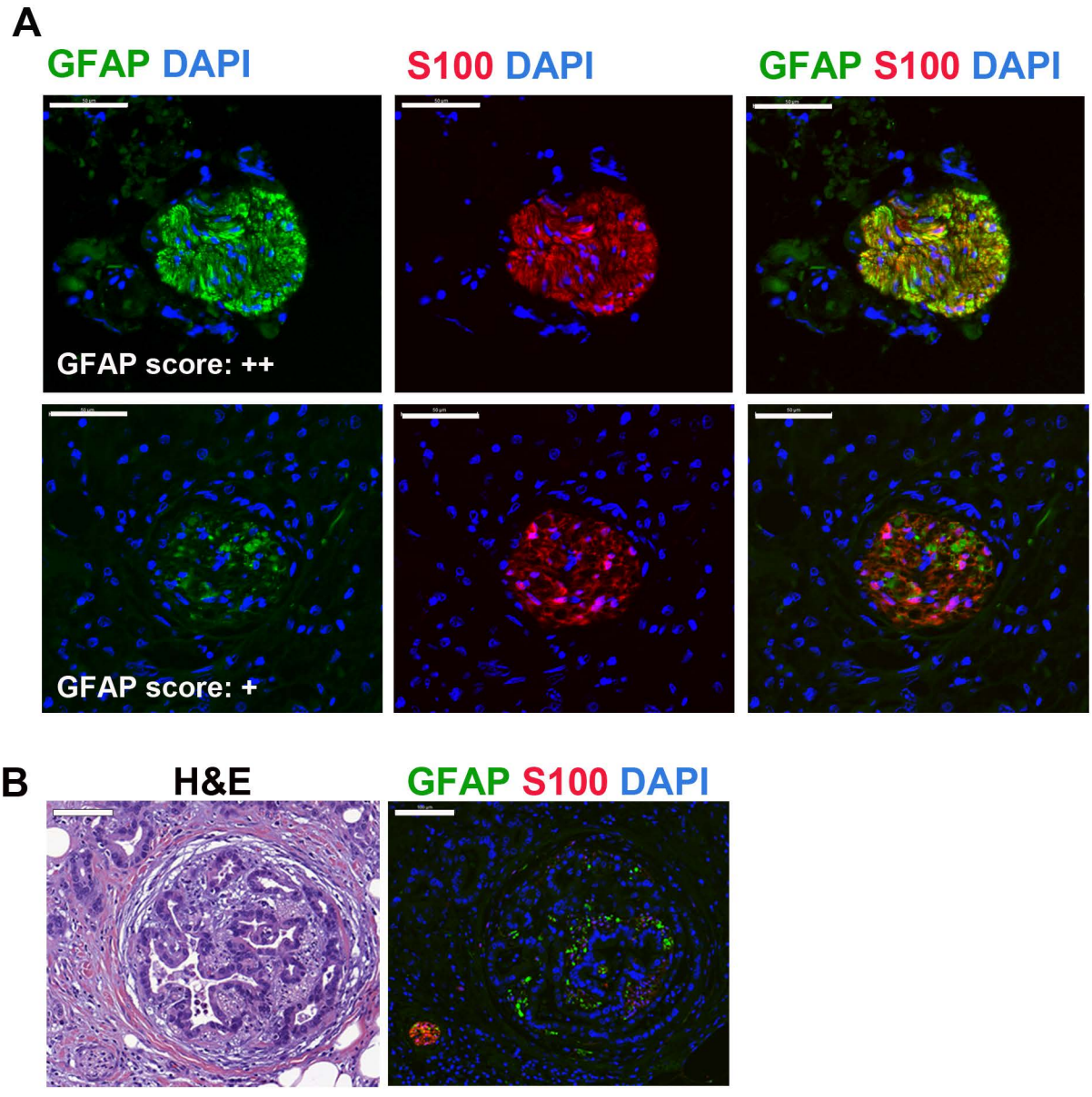

Supplementary Figure 1: GFAP positive nerves in patients with adenocarcinoma of the pancreas.
(A) Images of nerves stained for GFAP (green), S100 (red) and DAPI (blue), from patients with pancreatic adenocarcinomas, that score moderately (+) or highly (++) for GFAP. Scale bar: 50µm. (B) Table showing pathology reports of the 10 patients. (B) Images of an highly infiltrated nerve with GFAP (green) and S100 (red) staining, and corresponding H&E, showing almost complete disappearance of nerve tissue. Scale bar: 100µm.

Figure S2

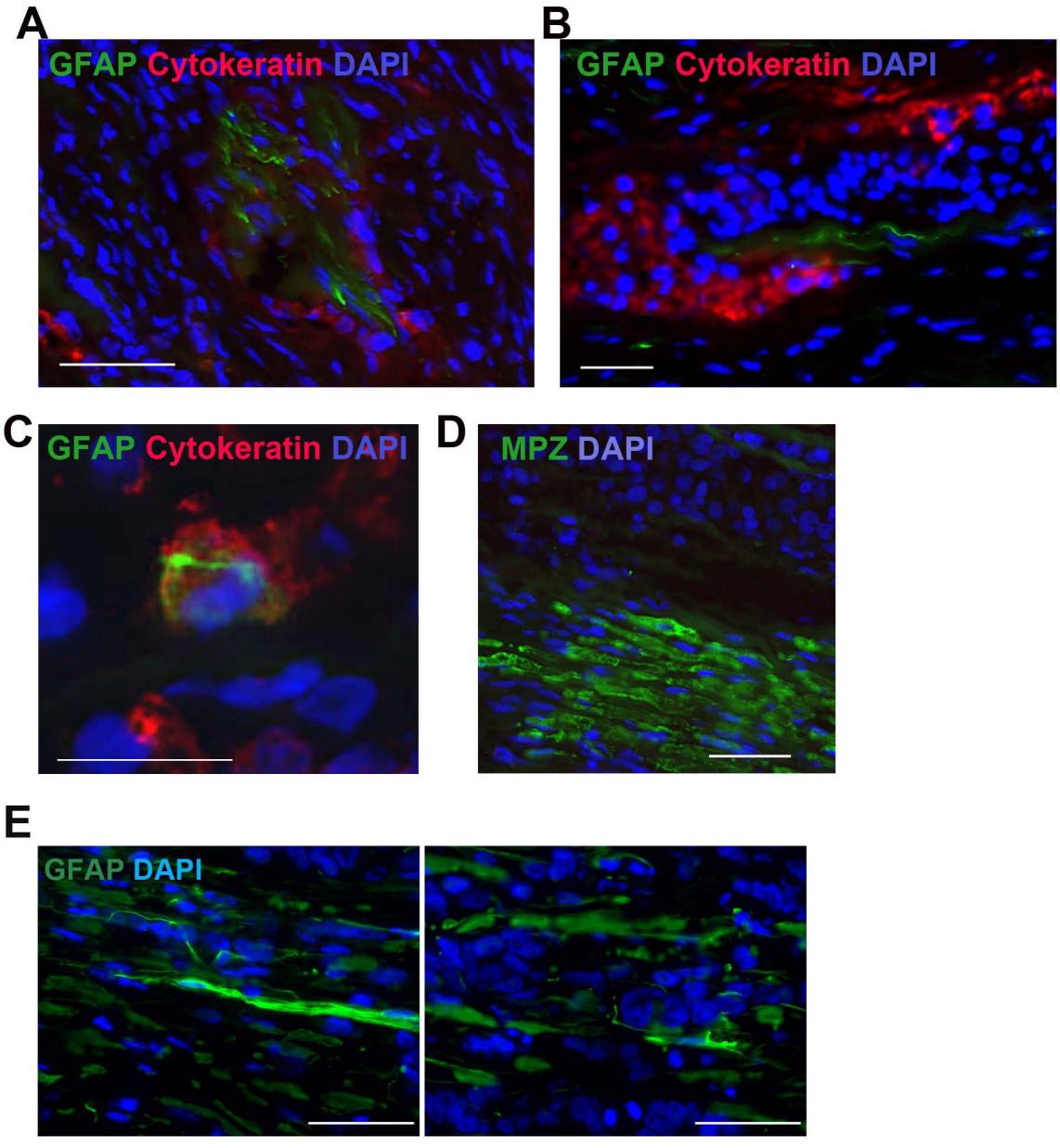

Supplementary Figure 2:GFAP+ Schwann cells are associated with cancer cells in vivo (human and mice specimen)

(A) GFAP+ Schwann cells are associated with cancer cells in a fragment of the facial nerve of a patient with salivary duct carcinoma. Scale bar: 50 µm. (B) GFAP+ Schwann cells are associated with cancer cells in a fragment of the infraorbital nerve of a patient with skin squamous cell carcinoma. Scale bar: 50 µm. (C) GFAP+ Schwann cells wrap individual cancer cells in a fragment of the recurrent laryngeal nerve of a patient with thyroid cancer. Scale bar: 20 µm. (D) Myelin Protein Zero+ Schwann cells are not associated with cancer cells in the patient with thyroid cancer. Scale bar: 50 µm. (E) GFAP+ Schwann cells with long processes are associated with injected MiaPaCa-2 cancer cells in a murine sciatic nerve. Scale bars: 50 µm.

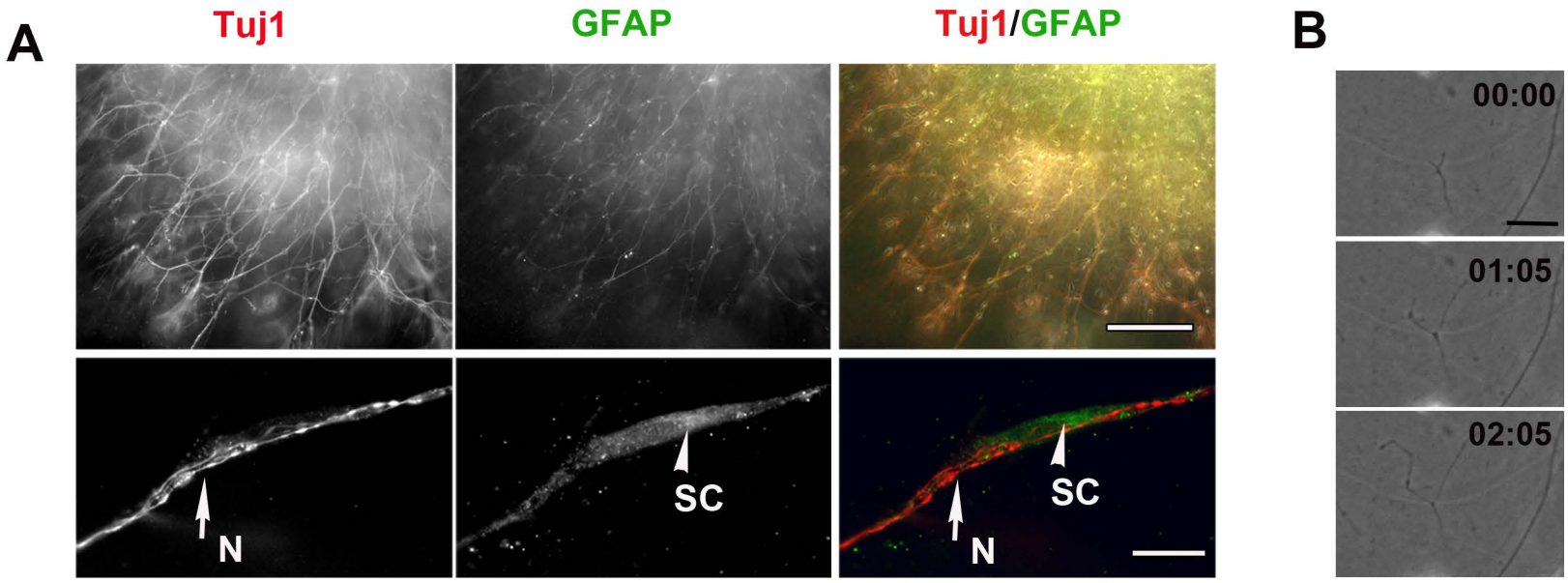

Supplementary Figure 3: Schwann cells are present along neurites in DRG and are not required for neurite growth. (A) Immunofluorescence staining for GFAP (green) and Tuj1 (red). The full arrow marks a neuron element and the arrowhead marks a Schwann cell. Scale bars are 200 μ m (upper image) and 20 μm (lower image). (B) Time lapse observations of a radiated DRG showing neurite growth. Images were taken every 5 min for 24h by phase contrast. Time is hours: minutes. Scale bar is 30 μm.

Figure S4

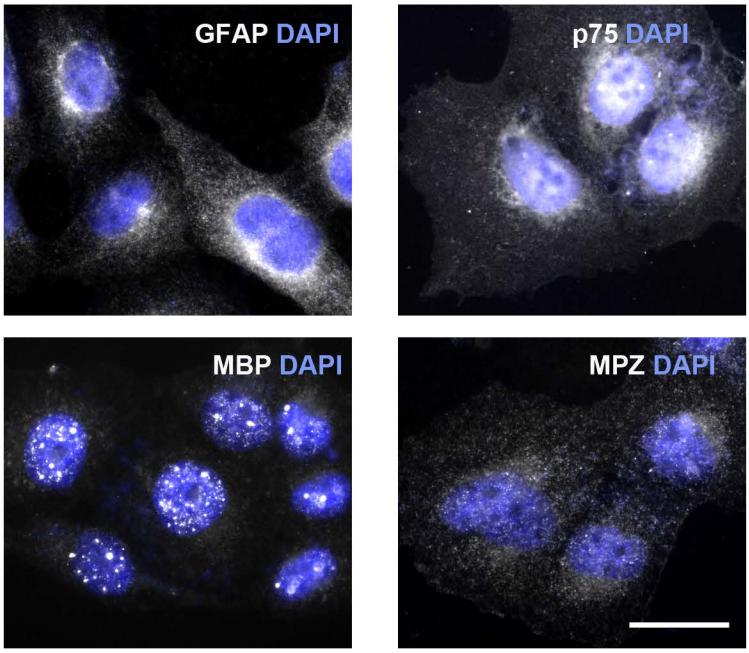

Supplementary Figure 4: Expression of Schwann cell markers in HEI-286 cells.
HEI-286 cells express both markers of Schwann cells involved in nerve repair (GFAP and p75) and markers of Schwann cells involved in myelination (MBP and MPZ). Immunofluorescence staining of GFAP, p75, MBP, and MPZ with nuclei staining (DAPI). Scale bars: 100 µm.

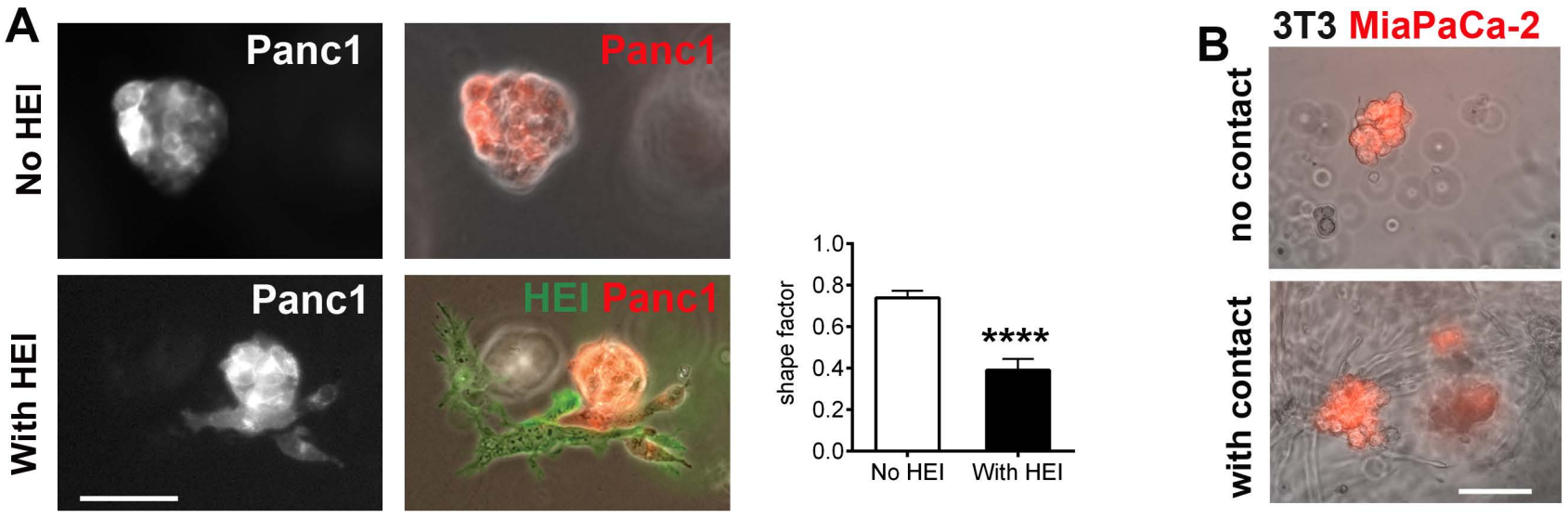

Supplementary Figure 5: Reorganization of cancer cell clusters
(A) Panc1 cancer cell clusters reorganize in presence of Schwann cells. Microscopic examination of organization of Panc1 cancer cells grown in Matrigel together with Schwann cells. Quantification of cancer cell reorganization using the shape factor index for Panc1 clusters growing with (HEI) or without (No HEI) HEI-286 Schwann cells. Data are means ± SEM. Significance was determined using t test (****$p<0.0001$, n (No HEI)=9, n (HEI)=7). (B) Microscopic examination of MiaPaCa-2 cell organization in Matrigel with NIH3T3. The cancer cell cluster shape is unaffected by contact with NIH3T3 (See quantification in Figure 6). Scale bars: 50 µm.

Figure S6

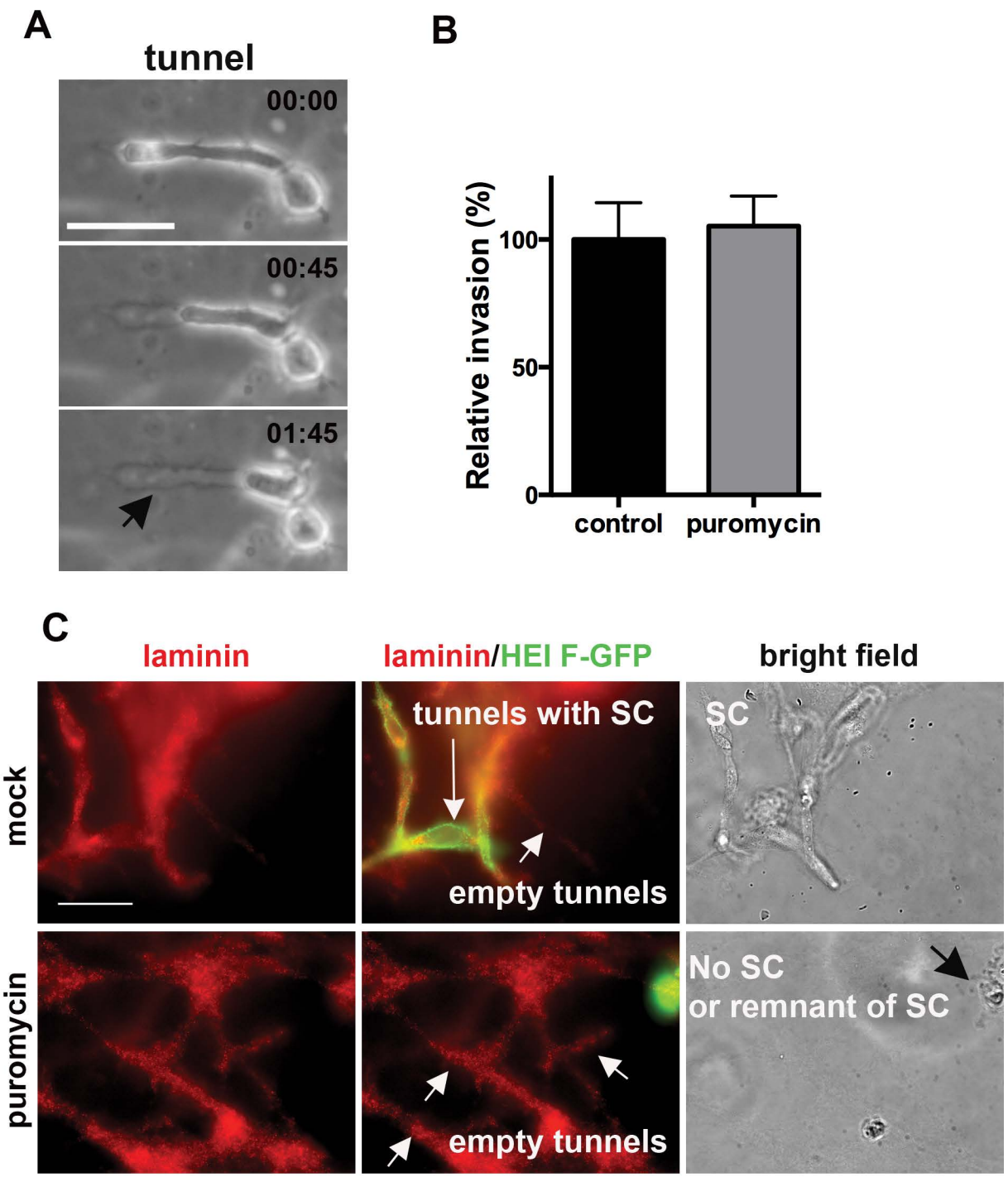

Supplementary Figure 6: Schwann cells form tunnels in Matrigel. (A) Time lapse images showing the formation of tunnels in Matrigel by the HEI-286 Schwann cell line. Arrow indicates tunnel after retraction of Schwann cells. Times are hours:minutes. (B) Puromycin treatment (3µg/ml) does not impair cancer invasion of puromycin resistant MiaPaCa-2 cancer cells in presence of puromycin resistant HEI-286 Schwann cell (control n=4, puromycin n=7, ns, t test). (C) Removal of non-puromycin resistant Schwann cells by puromycin treatment generates intact, empty tunnels. Immunofluorescence staining for laminin (red) and HEI-286 (F-GFP) in Matrigel samples that were mock (upper panels) or puromycin treated (lower panels). Small white arrows show empty tunnels, long arrow shows a tunnel with Schwann cells. Brightfield images (right) indicate absence or remnants (black arrow) of Schwann cells at location of tunnels. Scale bars: 50 µm.

Figure S7

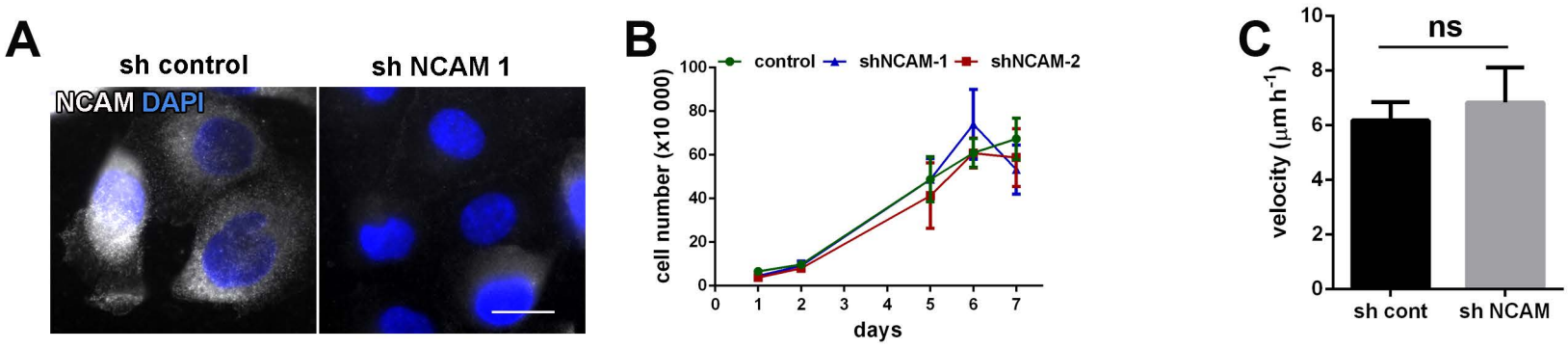

Supplementary Figure 7: Characterization of NCAM depleted HEI-286 Schwann cells
(A) Immunofluorescence staining for NCAM in control (sh) and NCAM depleted (sh NCAM1) HEI-286 cells. Scale bar: 20 µm. (B). Cell proliferation of control (sh), and NCAM depleted (shNCAM1 and shNCAM2) HEI-286 cells. Data are mean ± SD, n=3 for each data point. (C) Quantification of velocity of control (sh cont) and NCAM depleted (shNCAM) HEI-286 cells. Cells were seeded in insert (Ibidi) for 24h and allowed to migrate after removal of the insert. Velocity was calculated after measuring distance covered over a 24h period. Data are means ± SEM, n=7 for each cell type. Difference was not found significant, as determined using t test.

Figure S8

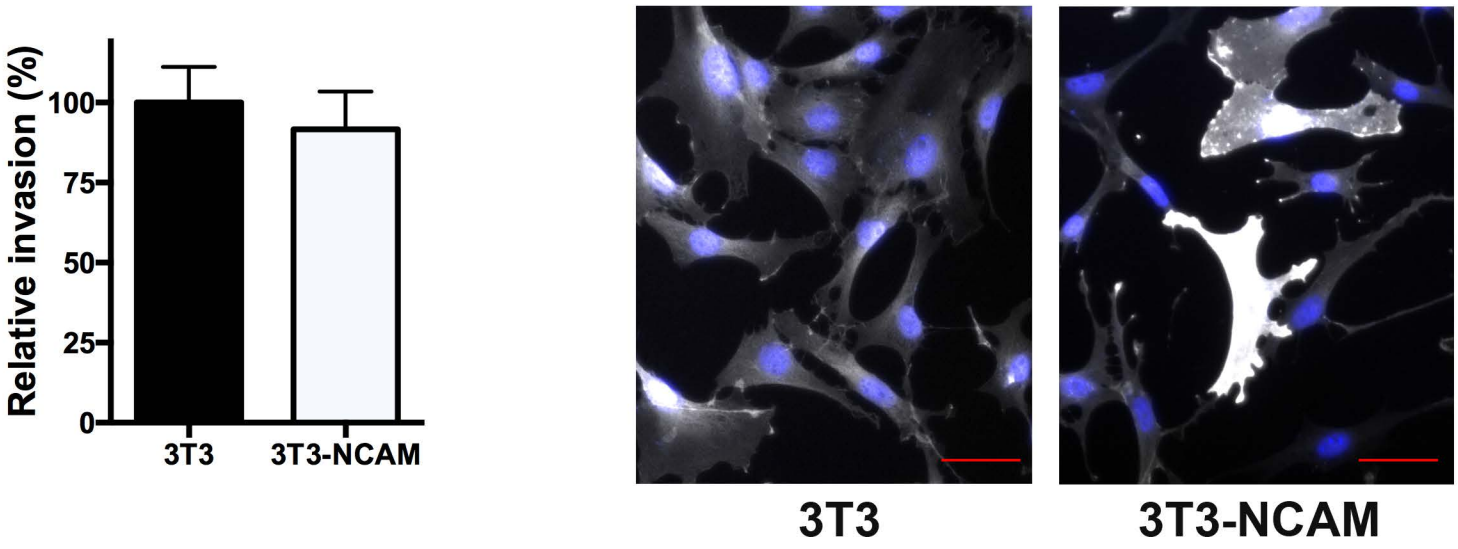

Supplementary Figure 8: Overexpression of NCAM in NIH 3T3 fibroblasts grown in Matrigel does not affect MiaPaCa-2 cells invasion.

Quantification of MiaPaCa-2 invasion in Matrigel grown with NIH 3T3 overexpressing NCAM or not. Data are means ± SEM, n=16 for each condition (2 experiments). No significant difference was found, as determined using t test. Microscopic images show overexpression of NCAM in 3T3 cells. Scale bar = 100µm.

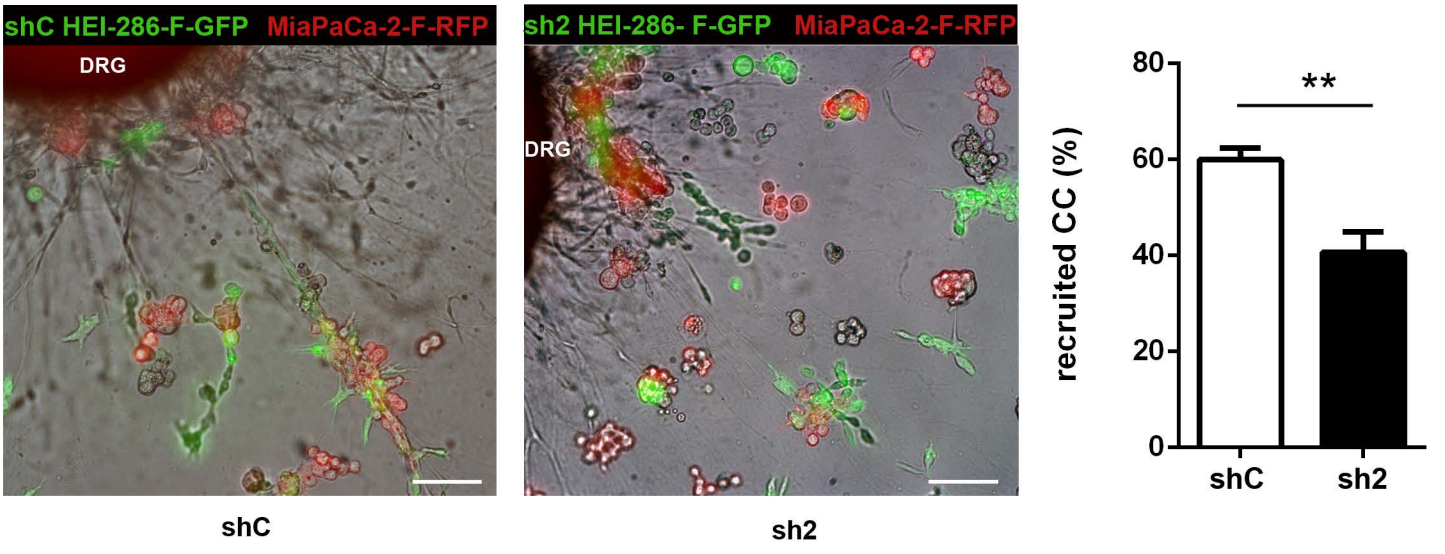

Supplementary Figure 9: NCAM depletion in Schwann cells reduced cancer cell recruitment to neurites of irradiated DRGs.
Irradiated DRGs were rescued with shNCAM HEI-286 (50,000cells) vs shcontrol HEI-286 6 days post radiation treatment, followed by the additional of MiaPaCa-2 cancer cells (50,000 cells) on day 7. Microscopic examination of the recruitment of cancer cells (red) to radiated DRGs and NCAM depleted Schwann cells (green). Images show MiaPaCa-2 (F-RFP) and HEI-286 (F-GFP) and were taken 10 days post irradiation. Quantification of the percentage of cancer cells that associated with the neurites in the presence of shC (n=13) and sh2 (n=16). Data are mean ± SEM. *P<0.05, **P<0.001, t test. Scale bars: 100μm.